INTERNATIONAL JOURNAL OF CONTROL
https://doi.org/10.1080/00207179.2025.2495124

Taylor & Francis
Taylor & Francis Group

Adaptive robust backstepping control based on radial basis neural network for linear motor drives

Paul Ager[a], Isah A. Jimoh [b], Geraint Bevan[a] and Ibrahim Küçükdemiral [a]

[a]Applied Instrumentation and Control, Department of Applied Science, Glasgow Caledonian University, Glasgow, UK; [b]Wind Energy and Control Centre, Department of Electronic and Electrical Engineering, University of Strathclyde, Glasgow, UK

ABSTRACT

This work presents an adaptive backstepping controller using a radial basis function neural network (RBF-NN) for position control of a linear motor drive with parameter uncertainties, discontinuous friction and unknown external disturbances. Initially, a robust control scheme is developed to ensure asymptotic stability. To avoid conservative tracking performance, we propose an adaptive robust backstepping law incorporating an RBF-NN to estimate lumped uncertainties and disturbances. The dynamic determination of the approximation error upper bound eliminates discontinuities in the adaptive control law. The RBF-NN's characteristics are utilised to establish the existence of solutions for the system, ensuring that the adaptive control law satisfies the Lipschitz continuity condition. The developed scheme ensures global asymptotic stability under bounded disturbances. Simulation results validate the proposed scheme's effectiveness in achieving precise positioning and reducing chattering compared to a robust backstepping controller, a fast nonsingular terminal sliding mode controller and an adaptive recursive terminal sliding mode controller.

ARTICLE HISTORY
Received 23 May 2024
Accepted 12 April 2025

KEYWORDS
Linear drive motor; adaptive backstepping control; model uncertainty; radial basis neural network

1. Introduction

Linear drive motors are widely used in modern manufacturing processes, including automatic machine inspection, machine tools, and semiconductor manufacturing (Z. Liu et al., 2024; Mirić et al., 2020; W. Wang et al., 2020). Their widespread adoption stems from advantages over rotary motors, such as the elimination of the need for gears between the motion device and motor, reduced mechanical loss, high operational speed, silent operation, and high initial thrust force (Paul et al., 2022). Despite these merits, linear drive motors exhibit a significant interaction between direct drives and the machining process (M. Yang et al., 2021), making it essential to develop drive control systems capable of delivering high tracking performance. Achieving a good tracking performance is challenging because motor parameters vary significantly due to the dynamics of the air gap, phase imbalance, rail resistivity, magnetisation saturation, and other factors (Wallscheid, 2021). Additionally, uncertain parameter variations, unmodelled dynamics, and external load disturbances further degrade the performance of the control system in practical applications (Gao et al., 2023; Nakata & Noda, 2023).

Frictional forces are unavoidable due to contact between surfaces in drive motor operation. These forces pose a major challenge to control systems by introducing steady-state error. Traditional methods, such as adaptive and variable-structure control (Y. Li et al., 2020; B. Zhang et al., 2020), address this issue by developing friction models to estimate and compensate for the effects of frictional forces. However, obtaining a precise friction model is difficult, as friction behaviour is usually not fully understood (Shao, Zheng, Wang, Wang, et al., 2021). Over the past three decades, extensive research has been conducted to overcome challenges like parameter variations and friction in linear drive motor position tracking control (Shi & Chen, 2023; Z. Wang et al., 2017; J. Zhang et al., 2020).

Various robust control schemes have been developed for linear drive motors. One approach is the use of feedforward control techniques to improve motor tracking performance. Yao and Xu (2002) highlighted that H_∞ methods often provide conservative performance, which is not ideal for high-accuracy tracking control. As an alternative, disturbance observer (DOB)-based controllers were proposed to enhance tracking performance in the face of system uncertainties (L. Li et al., 2020; Shao, Zheng, Wang, Xu, et al., 2021). Particularly, L. Li et al. (2020) developed a two-degree-of-freedom (2-DOF) H_∞ control system that combines an H_∞ disturbance observer with feedback and feedforward controllers to enhance robustness and dynamic response while providing robust tracking. An experimental study (X. Wang et al., 2021) demonstrated that the DOB approach cannot adequately manage the discontinuities associated with Coulomb friction. Another factor driving the development of position controllers for linear motor drives is the need to minimise nonlinear ripple and cogging effects. For instance, a first-order approximation of ripple effects was experimentally obtained, upon which a feedforward controller was developed to cancel these effects, thus improving position tracking (Van Den Braembussche et al., 1996). However, this

CONTACT Isah A. Jimoh isah.jimoh@strath.ac.uk, rashman9ja@gmail.com Wind Energy and Control Centre, Department of Electronic and Electrical Engineering, University of Strathclyde, Glasgow G1 1XW, UK

offline technique of identifying a compensation model can be of limited utility since it may change due to operating conditions, and a particular model may only be useful for a specific linear drive motor. In light of this, a feedforward controller that relies on neural networks to estimate uncertainties was proposed to improve positional accuracy (Otten et al., 1997). However, this scheme, which relied on a neural network (NN), did not provide a theoretical guarantee of closed-loop stability. In a recent study (Shi & Chen, 2023), a fractional-order ideal cut-off Bode filter was used to suppress the effects of high-frequency noise and an extended state observer was used to implement a feed-forward control system for a linear motor drive system.

Given the weaknesses associated with the above control methods, adaptive robust control (ARC) methods have garnered significant interest in position-tracking control of linear motors. These ARC schemes mostly rely on backstepping techniques that utilise Lyapunov functions to enforce the asymptotic stability of the closed-loop response of the drive motors. Adaptive backstepping is achieved via a recursive and systematic design procedure for nonlinear feedback control, providing a structured approach to handling system uncertainties and nonlinearities (Yu et al., 2020). For instance, Yuan et al. (2019) developed a dual-loop control strategy to improve the speed and tracking accuracy of the linear drive system. The outer loop implemented an online trajectory replanning strategy that forces the replanned trajectory to converge to the actual trajectory in minimum time under system constraints. The inner loop then employed an ARC to improve tracking performance under disturbances. The control framework's performance was experimentally validated.

An ARC scheme was developed for high-speed and high-accuracy position control of machine tools driven by rotary AC motors (Gai et al., 2021). By leveraging the Lyapunov stability theory, the researchers designed an adaptive law and validated the control strategy through simulation and experiments. The results demonstrated significant improvements in motion control accuracy, response speed, and noise suppression. Additionally, significant disturbances and parameter variations are accommodated in the ARC technique as opposed to the DOB method, whose performance can degrade markedly when estimation accuracy declines. Shao, Zheng, Wang, Wang, et al. (2021) developed an ARC for iron-core linear motors, which exhibit greater parameter variations and other difficulties when compared to their rotary counterparts. The effectiveness of the scheme was demonstrated via extensive simulation studies. Z. Liu et al. (2023) developed an ARC for linear motor-driven systems using a gradient descent-based B-spline wavelet neural network compensator. The proposed control scheme integrated recursive least squares (RLS)-based parameter estimation, a neural network compensator to estimate complex uncertainties, and an anti-saturation auxiliary system. The experimental results showed improved tracking accuracy, optimal parameter estimation, and effective compensation for actuator saturation, making the method highly suitable for real-time, high-precision applications in linear motor systems.

The sliding mode control (SMC) strategy has garnered significant attention due to its ability to enhance the robustness of control systems for linear motor drives (X. Sun et al., 2023). SMC has been proven effective in mitigating the adverse effects of model inaccuracies and external disturbances, which are common challenges in high-precision applications (Mousavi et al., 2023). By maintaining stability and performance even under uncertain conditions, sliding mode control has emerged as a preferred technique for ensuring reliable and accurate operation in demanding environments. Tu and Dong (2023) developed a dual-layer SMC framework for the robust control of linear motor drive systems in the presence of actuator faults and external disturbances. The method integrated an integral sliding function with an auxiliary controller to handle time derivatives and introduced a nested sliding mode to decouple disturbances, ensuring uniformly bounded system responses. Simulations demonstrated superior tracking accuracy, robustness, and reduced chattering compared to conventional SMC methods.

An experimental study (G. Sun et al., 2018) proposed a fractional-order SMC strategy for the linear motor drive to improve its robustness in the presence of model uncertainties and external disturbances. Shao, Zheng, Wang, Wang, et al. (2021) proposed a barrier function adaptive SMC scheme to address issues with conventional robust SMC methods, which often exhibit chattering under low-disturbance conditions. This approach adjusts the controller gain based on disturbance magnitude to reduce chattering and optimise control effort (Shao, Zheng, Wang, Wang, et al., 2021). Experimental results demonstrated its effectiveness in linear motor positioning control.

In light of the reviewed literature, ensuring accurate and reliable position tracking in linear motor drive systems remains a challenging task due to various inherent and external factors. The primary challenges in controlling linear motor drives arise from significant parameter variations caused by factors such as air gap dynamics, phase imbalances, and magnetic saturation. These uncertainties are further compounded by unmodelled dynamics and external disturbances, including load changes and environmental effects. Frictional forces, particularly discontinuous types such as Coulomb and stiction friction, add another layer of complexity, often leading to steady-state errors and oscillations, thereby degrading system performance. Conventional control methods, while effective to a degree, struggle to address these multifaceted challenges (Xu et al., 2018).

Robust control strategies, for instance, typically rely on conservatively predefined disturbance bounds, which can result in suboptimal tracking performance (Mohanraj et al., 2022). Adaptive control methods, on the other hand, often require detailed friction models or precise system characterisation, which are difficult to develop and may not generalise across different operational conditions. In a recent study (Ager et al., 2024), it was demonstrated that an adaptive mechanism can enhance the performance of a conventional backstepping controller by leveraging delayed state and input variables to approximate the upper bound of the disturbance. However, this approach attempts to estimate the upper bound of the previous disturbance in the current time, leading to a discontinuous control law with significant chattering effects in the control input.

Motivated by the limitations of conventional robust and sliding mode controllers, which rely on discontinuous laws, for

instance, sgn(·) functions, and predefined bounds, often resulting in chattering (Zheng et al., 2015), this study introduces an adaptive robust backstepping control (AR-BSC) strategy enhanced with a radial basis function neural network (RBF-NN).

Leveraging the RBF-NN's universal approximation capability, our approach smoothly estimates nonlinear uncertainties, adaptively adjusts the approximation error bound to eliminate conservative limits, and ensures a continuous control law without online weight tuning. This integration of adaptive learning and robust control delivers precise position tracking, significantly reduced chattering, and global asymptotic stability, outperforming traditional methods in handling diverse, dynamic uncertainties, as validated by comprehensive simulations–offering a critical advancement for high-precision linear motor applications.

The main contributions of this study are as follows:

- This work introduces a novel adaptive robust backstepping control strategy that combines the universal approximation capability of RBF-NNs with a robust control law to effectively handle parameter uncertainties, external disturbances, and discontinuous frictional forces.
- The proposed scheme employs a combination of an RBF-NN and an adaptive estimation of error bounds to eliminate discontinuities in the control law and reduce input chattering, thereby ensuring smoother and more stable control performance compared to existing robust and sliding-mode controllers.
- The proposed control law is shown to be Lipschitz continuous and globally asymptotically stabilising under the given assumptions.
- Comprehensive simulations demonstrate that the proposed controller outperforms conventional methods, including robust backstepping, fast terminal nonsingular sliding mode control (FTNSMC), and adaptive recursive terminal sliding mode control (ARTSMC), achieving superior tracking accuracy and significantly reduced chattering.

The rest of this paper is organised as follows. Section 2 presents the formulation of the problem by describing the mathematical model of the linear motor and stating the control objective. Section 3 provides the development of a robust backstepping controller with a sign function and the neural-network-based adaptive robust backstepping scheme. An extensive simulation studies are presented in Section 4. Finally, Section 5 provides concluding remarks.

Notation: We adopt standard notation throughout this text. The operator $\|\cdot\|$ denotes the 2-norm of its argument. We simply denote $\frac{dx}{dt}$ by $\dot{x}$. For brevity, time dependence of time-varying signals is omitted unless explicitly required.

2. Preliminaries

2.1 Linear drive motor model

The linear drive system with parameter deviations and external disturbances can be modelled as:

$$\dot{x}_1 = x_2$$

$$M\dot{x}_2 = k_f u - (B + \Delta B)x_2 - f(x_2) - f_d \tag{1}$$

where x_1 [m] is the position of the mover, x_2 [m/s] is the mover velocity. We define $x \triangleq [\, x_1 \; x_2 \,]^\top$ as the state vector, M [kg] is the total mass of the moving element, B [Ns/m] represents the combined viscous friction coefficient and load damping, ΔB is a parametric uncertainty, f_d [N] represents the external disturbance force, u [V] is the control input voltage of the motor, while k_f [N/V] is the input constant. In addition, $f(x_2)$ [N] is the combined stiction and Coulomb friction. By considering the Coulomb, stiction, and Stribeck effect, this is expressed as F. J. Lin et al. (2002):

$$f(x_2) = f_c \,\mathrm{sgn}(x_2) + (f_s - f_c)\exp\{-(x_2/\dot{x}_s)^2\}\,\mathrm{sgn}(x_2) + K_v x_2, \tag{2}$$

where f_c is the Coulomb friction, f_s is the static friction, $\dot{x}_s$ denotes the Stribeck velocity parameter, sgn(·) is the sign function, and K_v is the viscous coefficient.

The model (1) can be re-written with lumped uncertainties and disturbances as follows:

$$\begin{aligned} \dot{x}_1 &= x_2 \\ \dot{x}_2 &= \bar{A}x_2 + \bar{B}u + \bar{C}(f(x_2) + F_{e,1}) \\ y &= x_1 \end{aligned} \tag{3}$$

y is the controlled output, $\bar{A} = -B/M$, $\bar{B} = k_f/M$, $\bar{C} = -1/M$, and $F_{e,1} = \Delta B x_2 + f_d$ represents the system uncertainty, which includes parameter uncertainty and unknown exogenous disturbance, f_d. The exogenous disturbance f_d is unknown but bounded and must be observed. Observing the unknown disturbance is underpinned by the assumption that the disturbance remains constant during the observation period. This is a practical assumption in real applications where the observer's update rate exceeds the disturbance's (f_d) variation rate, as is common in high-speed control systems.

2.2 Problem formulation

The primary objective of this study is to design a control system for the linear motor drive, modelled by (1)–(3), that ensures precise position tracking despite significant challenges posed by parameter uncertainties, discontinuous frictional forces, and unknown external disturbances. Specifically, let y^d denote the desired reference position trajectory, which may differ from the initial mover position $x_1(t_0)$. The control problem is to synthesise a control input u such that the mover position $y = x_1$ asymptotically tracks the reference trajectory, i.e.

$$\lim_{t\to\infty} |y(t) - y^d(t)| = 0,$$

while maintaining stability and smoothness in the presence of the following challenging factors:

(1) *Parameter Uncertainties*: The viscous friction coefficient B is subject to variations ΔB, reflecting changes due to air gap dynamics, phase imbalances, or operating conditions, which introduce uncertainty in the system dynamics (Wallscheid, 2021).

(2) *Discontinuous Frictional Forces*: The friction term $f(x_2)$, defined in Equation (2), includes Coulomb and stiction components with sign functions and Stribeck effects, rendering the system nonlinear and discontinuous (F. J. Lin et al., 2002).
(3) *Unknown External Disturbances*: The exogenous disturbance f_d is bounded but unknown, varying unpredictably in practical applications (e.g. load changes), and must be compensated without precise prior knowledge (Gao et al., 2023).

These factors collectively degrade tracking performance, introduce steady-state errors, and can lead to undesirable chattering in the control input–issues that conventional robust control methods struggle to address effectively due to their reliance on conservative disturbance bounds or discontinuous laws (e.g. $\text{sgn}(\cdot)$).

Traditional robust backstepping control (R-BSC), as explored in Section 3.2, employs a sign function to bound uncertainties (e.g. $|F_{e,1}| \leq \bar{F}_e$), achieving stability but at the cost of discontinuities that violate Lipschitz conditions and induce chattering (Remark 3.2). This motivates an adaptive approach leveraging the universal approximation capability of radial basis function neural networks (RBF-NNs) to estimate the lumped uncertainty $f_1(x_2) = f(x_2) + F_{e,1} - K_v x_2$ (where $K_v x_2$ is known and excluded from estimation) as a continuous function $d(x)$, with an approximation error defined as:

$$\epsilon(t) \triangleq f_1(x_2) - d(x). \tag{4}$$

To ensure the feasibility of this approach, we introduce the following assumptions:

Assumption 2.1: *Considering the universal approximation property of RBF-NNs, which can approximate arbitrary nonlinear and discontinuous functions with bounded errors (H. Yang & Liu, 2018), the approximation error $\epsilon(t)$ is bounded such that $|\epsilon(t)| \leq \bar{\epsilon}$ for all t with $\bar{\epsilon}$ being an adaptive bound. The boundedness of $\epsilon(t)$ is supported by the fact that $f_1(x_2)$ is constructed from physically measurable and bounded phenomena, such as Coulomb friction and external disturbances.*

Assumption 2.2: (a) *There exists a continuous function*

$$d(x) = K_1 \exp\{-(x - x_c)^\top Q(x - x_c)\}, \tag{5}$$

with $Q \in \mathbb{R}^{2\times 2}$ positive definite, $K_1 \in \mathbb{R}$, and $x_c \in \mathbb{R}^2$, that approximates $f_1(x_2)$.

(b) *The control signal $u(x)$ for the system (3) is Lipschitz continuous, i.e. $\|u(x) - u(\tilde{x})\| \leq L_u \|x - \tilde{x}\|$, where $L_u > 0$ is the Lipschitz constant (Gwiazda et al., 2010).*

Under these assumptions, let us rewrite the system dynamics (3) as:

$$F(t, x, u) \triangleq \begin{bmatrix} x_2 \\ \bar{A}x_2 + \bar{B}u + \bar{C}K_v x_2 + \bar{C}d(x) + F_{e,2} \end{bmatrix}, \tag{6}$$

where $F_{e,2}$ accounts for the scaled the approximation error. The control problem thus reduces to designing an adaptive robust backstepping control (AR-BSC) law $u(x)$ that: (i) ensures $F(t, x, u)$ satisfies a Lipschitz condition for solution existence (Theorem 3.1), (ii) adaptively estimates $d(x)$ and $\bar{\epsilon}$ to eliminate discontinuities in the control law, and (iii) guarantees global asymptotic stability of the tracking error z_1. Theorem 3.1, proven below, establishes the theoretical foundation.

3. Main results

3.1 Existence and uniqueness of the solution

The adaptive robust backstepping control (AR-BSC) design ensures that the system dynamics $\dot{x} = F(t, x, u)$ (Equation (6)) exhibit continuity and Lipschitz properties, critical in the presence of nonlinearities such as discontinuous friction and external disturbances. The Lipschitz condition on $F(t, x, u)$ bounds its rate of change with respect to x, guaranteeing a unique solution via the Picard-Lindelöf theorem (Walter, 2013) and reflecting smooth operation of the linear motor drive. The radial basis function neural network (RBF-NN) approximates lumped uncertainties (e.g. Coulomb friction and disturbances) as a continuous function $d(x)$, while the control input $u(x)$ employs smooth approximations to avoid destabilising discontinuities. Under Assumptions 2.1 and 2.2, the Picard-Lindelöf theorem applies, establishing solution existence for Equation (6). The Lipschitz continuity of $u(x)$, ensured by the proposed control's design and bounded adaptive components, aligns with recent studies on nonlinear systems (e.g. W. Wang, Wu, et al., 2025; W. Wang, Zeng, et al., 2025), reinforcing the theoretical and practical significance of these conditions for stability and predictability.

Theorem 3.1: *Under Assumptions 2.1 and 2.2, $F(t, x, u)$ is a vector-valued continuous function that satisfies the Lipschitz condition:*

$$\|F(t, x, u) - F(t, \tilde{x}, \tilde{u})\| \leq L\|x - \tilde{x}\| \tag{7}$$

for all $x, \tilde{x} \in \mathcal{B}(x_0, r) \triangleq \{x \in \mathbb{R}^2 : \|x - x_0\| \leq r\}$ with $t \in [t_0, t]$. Then, there exists $\delta > 0$ such that the state equation $\dot{x} = F(t, x, u)$ with the initial condition $x(t_0) = x_0$ has a unique solution over $[t, t + \delta]$.

Proof: Given Assumptions 2.1 and 2.2, we first show that the function $F(t, x, u)$ satisfies the Lipschitz continuity condition with respect to the state variable x. This implies there exists a constant $L > 0$, such that for all $x, \tilde{x} \in \mathcal{B}(x_0, r)$, the (7) holds.

Let us first calculate $d_F \triangleq F(t, x, u) - F(t, \tilde{x}, \tilde{u})$:

$$d_F = \begin{bmatrix} x_2 - \tilde{x}_2 \\ (\bar{A} + \bar{C}K_v)(x_2 - \tilde{x}_2) + \bar{B}(u - \tilde{u}) + \bar{C}(d(x) - d(\tilde{x})) \end{bmatrix}. \tag{8}$$

Given Assumption 2.1, the bounded approximation error $\epsilon(t)$ does not affect the Lipschitz continuity of $F(t, x, u)$, since it only represents a bounded additive term. Thus, using the triangle inequality and norm properties, we have:

$$\|F(t, x, u) - F(t, \tilde{x}, \tilde{u})\| \leq \|x_2 - \tilde{x}_2\| + \|(\bar{A} + \bar{C}K_v)(x_2 - \tilde{x}_2)\| + \|\bar{B}(u - \tilde{u})\| + \|\bar{C}(d(x) - d(\tilde{x}))\|$$

$$\leq \left(1 + \|\bar{A} + \bar{C}K_v\|\right) \|x_2 - \tilde{x}_2\| + \|\bar{B}\|\|u - \tilde{u}\| + \|\bar{C}\|\|d(x) - d(\tilde{x})\|. \tag{9}$$

Given that the control input $u(x)$ satisfies Assumption 2.1, we have:

$$\|u - \tilde{u}\| \leq L_u \|x - \tilde{x}\|. \tag{10}$$

To estimate the Lipschitz constant L_f associated with the continuous function $d(x)$, we apply the mean value theorem for vector-valued functions. Thus, there exists a vector ξ on the line segment connecting x and $\tilde{x}$ such that:

$$d(x) - d(\tilde{x}) = \nabla d(\xi)(x - \tilde{x}), \tag{11}$$

where the gradient $\nabla d(x)$ is given by:

$$\nabla d(x) = K_1 \exp\left\{-(x - x_c)^\top Q(x - x_c)\right\} (-2Q(x - x_c)).$$

Since $Q \in \mathbb{R}^{2\times 2}$ is positive definite, the exponential term satisfies:

$$0 \leq \exp\left\{-(x - x_c)^\top Q(x - x_c)\right\} \leq 1. \tag{12}$$

Therefore, the gradient norm is bounded as follows:

$$\begin{aligned}\|\nabla d(\xi)\| &\leq 2\|K_1\|\|Q\|\|\xi - x_c\| \exp\left\{-(\xi - x_c)^\top Q(\xi - x_c)\right\} \\ &\leq 2\|K_1\|\lambda_{\max}(Q) \sup_{\xi \in \mathcal{B}(x_0, r)} \|\xi - x_c\|. \end{aligned} \tag{13}$$

where $\lambda_{\max}(Q)$ stands for the maximum eigenvalue of Q. Hence, we have the following bound on the difference:

$$\|d(x) - d(\tilde{x})\| \leq L_f \|x - \tilde{x}\|, \tag{14}$$

where the Lipschitz constant L_f is defined as:

$$L_f = 2\|K_1\|\lambda_{\max}(Q) \sup_{\xi \in \mathcal{B}(x_0, r)} \|\xi - x_c\|.$$

Therefore, considering bounds (10) and (14), we conclude:

$$\|F(t, x, u) - F(t, \tilde{x}, \tilde{u})\| \leq L\|x - \tilde{x}\|, \tag{15}$$

where the Lipschitz constant L is given by:

$$L = 1 + \|\bar{A} + \bar{C}K_v\| + \|\bar{B}\|L_u + \|\bar{C}\|L_f.$$

Consequently, since $F(t, x, u)$ satisfies the Lipschitz condition in x, by the Picard–Lindelöf theorem, the local existence and uniqueness of the solution to the initial-value problem $\dot{x} = F(t, x, u)$ with initial condition $x(t_0) = x_0$ is guaranteed within a neighbourhood of x_0, on the time interval $[t_0, t_0 + \delta]$. This concludes the proof. ■

3.2 Robust backstepping control system

The design of a robust backstepping controller (R-BSC) for the nonlinear discontinuous system (3) is presented in this section. The objective is to achieve precise position tracking by steering the tracking error z_1, defined as

$$z_1 \triangleq y - y^d, \tag{16}$$

towards zero, where $y = x_1$ is the mover position and y^d is the desired reference trajectory. The derivative of the tracking error is

$$\dot{z}_1 = x_2 - \dot{y}^d, \tag{17}$$

since $\dot{x}_1 = x_2$ from (1). Here, the state x_2 (velocity) is treated as a virtual control input. Let us define the stabilising function:

$$\eta \triangleq \dot{y}^d - k_1 z_1, \tag{18}$$

where $k_1 > 0$ is a design constant. If $x_2 = \eta$, then

$$\dot{z}_1 = x_2 - \dot{y}^d = (\dot{y}^d - k_1 z_1) - \dot{y}^d = -k_1 z_1. \tag{19}$$

Now let us consider the first Lyapunov function:

$$V_1 \triangleq \frac{1}{2} z_1^2. \tag{20}$$

Its time-derivative, under the condition $x_2 = \eta$, is

$$\dot{V}_1 = z_1 \dot{z}_1 = z_1(-k_1 z_1) = -k_1 z_1^2. \tag{21}$$

Since $k_1 > 0$, $\dot{V}_1$ is globally negative definite, indicating that z_1 would be asymptotically stable if $x_2 = \eta$ holds. However, x_2 is a state, not a control input, so define the secondary error:

$$z_2 \triangleq x_2 - \eta. \tag{22}$$

Thus, $x_2 = z_2 + \eta$, and

$$\begin{aligned}\dot{z}_1 &= x_2 - \dot{y}^d \\ &= (z_2 + \eta) - \dot{y}^d \\ &= z_2 + (\dot{y}^d - k_1 z_1) - \dot{y}^d \\ &= z_2 - k_1 z_1 \end{aligned} \tag{23}$$

The derivative of z_2 is

$$\begin{aligned}\dot{z}_2 &= \dot{x}_2 - \dot{\eta}, \\ &= \bar{A}x_2 + \bar{B}u + \bar{C}f(x_2) + \bar{C}F_{e,1} - \dot{\eta}, \end{aligned} \tag{24}$$

where, from (3), $\dot{x}_2 = \bar{A}x_2 + \bar{B}u + \bar{C}f(x_2) + \bar{C}F_{e,1}$, and

$$\dot{\eta} = \ddot{y}^d - k_1 \dot{z}_1 = \ddot{y}^d - k_1(x_2 - \dot{y}^d). \tag{25}$$

To account for parametric uncertainties and disturbances, assume the lumped uncertainty $F_{e,1}$ is bounded such that $|F_{e,1}| \leq \bar{F}_e$, where $\bar{F}_e > 0$ is a known constant.

Define the second Lyapunov function:

$$V_2(z_1, z_2) \triangleq V_1 + \frac{1}{2} z_2^2 = \frac{1}{2} z_1^2 + \frac{1}{2} z_2^2. \tag{26}$$

Its time-derivative yields

$$\begin{aligned}\dot{V}_2(z_1,z_2) &= z_1\dot{z}_1 + z_2\dot{z}_2,\\ &= z_1(z_2 - k_1 z_1)\\ &\quad + z_2\left[\bar{A}x_2 + \bar{B}u + \bar{C}f(x_2) + \bar{C}F_{e,1} - \dot{\eta}\right],\\ &= -k_1 z_1^2 + z_1 z_2\\ &\quad + z_2\left[\bar{A}x_2 + \bar{B}u + \bar{C}f(x_2) + \bar{C}F_{e,1} - \dot{\eta}\right]. \end{aligned} \tag{27}$$

Now we can propose the following robust backstepping control law:

$$u = \bar{B}^{-1}\left[-k_2 z_2 - z_1 - \bar{A}x_2 - \bar{C}f(x_2) + \bar{C}\bar{F}_e \mathrm{sgn}(z_2) + \dot{\eta}\right], \tag{28}$$

where $k_2 > 0$ is a design constant, and the term $-z_1$ cancels the cross-term $z_1 z_2$ in $\dot{V}_2$, while $\bar{C}\bar{F}_e\mathrm{sgn}(z_2)$ (with $\bar{C} = -1/M < 0$) compensates for the disturbance $\bar{C}F_{e,1}$. Then, substituting (28) into (24) gives

$$\begin{aligned}\dot{z}_2 &= \bar{A}x_2 + (-k_2 z_2 - z_1 - \bar{A}x_2 - \bar{C}f(x_2) + \bar{C}\bar{F}_e\mathrm{sgn}(z_2) + \dot{\eta})\\ &\quad + \bar{C}f(x_2) + \bar{C}F_{e,1} - \dot{\eta}\\ &= -k_2 z_2 - z_1 + \bar{C}(F_{e,1} + \bar{F}_e\mathrm{sgn}(z_2)) \end{aligned} \tag{29}$$

Now, substituting $\dot{z}_2$ into $\dot{V}_2$ results in

$$\begin{aligned}\dot{V}_2 &= z_1(z_2 - k_1 z_1)\\ &\quad + z_2\left[-k_2 z_2 - z_1 + \bar{C}(F_{e,1} + \bar{F}_e\mathrm{sgn}(z_2))\right]\\ &= -k_1 z_1^2 + z_1 z_2 - k_2 z_2^2 - z_1 z_2 + z_2\bar{C}(F_{e,1} + \bar{F}_e\mathrm{sgn}(z_2))\\ &= -k_1 z_1^2 - k_2 z_2^2 + z_2\bar{C}(F_{e,1} + \bar{F}_e\mathrm{sgn}(z_2)). \end{aligned} \tag{30}$$

Let us focus on the robust term with $\bar{C} = -1/M < 0$:

$$z_2\bar{C}(F_{e,1} + \bar{F}_e\mathrm{sgn}(z_2)) = -\frac{z_2}{M}(F_{e,1} + \bar{F}_e\mathrm{sgn}(z_2)), \tag{31}$$

Note that

- If $z_2 > 0$: $\mathrm{sgn}(z_2) = 1$, $F_{e,1} + \bar{F}_e \geq F_{e,1} - |F_{e,1}| \geq 0$, so $-\frac{z_2}{M}(F_{e,1} + \bar{F}_e) \leq 0$,
- If $z_2 < 0$: $\mathrm{sgn}(z_2) = -1$, $F_{e,1} - \bar{F}_e \leq |F_{e,1}| - \bar{F}_e \leq 0$, so $-\frac{z_2}{M}(F_{e,1} - \bar{F}_e) \leq 0$,
- If $z_2 = 0$: the term is zero.

Thus:

$$\begin{aligned}\dot{V}_2(z_1,z_2) &= -k_1 z_1^2 - k_2 z_2^2 + z_2\bar{C}(F_{e,1} + \bar{F}_e\mathrm{sgn}(z_2)),\\ &\leq -k_1 z_1^2 - k_2 z_2^2,\\ &\leq 0, \end{aligned} \tag{32}$$

Let us define

$$D(t) \triangleq k_1 z_1^2 + k_2 z_2^2 \leq -\dot{V}_2(z_1(t), z_2(t)). \tag{33}$$

Integrating both sides from 0 to t yields

$$\int_0^t D(\tau)\,\mathrm{d}\tau \leq V_2(z_1(0), z_2(0)) - V_2(z_1(t), z_2(t)). \tag{34}$$

Since $V_2 \geq 0$ and $\dot{V}_2 \leq 0$, $V_2(t)$ is non-increasing and bounded, implying:

$$\lim_{t\to\infty}\int_0^t D(\tau)\,\mathrm{d}\tau \leq V_2(z_1(0), z_2(0)) < \infty. \tag{35}$$

To apply Barbalat's lemma, let us check the uniform continuity of $D(t)$. Compute:

$$\dot{D}(t) = 2k_1 z_1\dot{z}_1 + 2k_2 z_2\dot{z}_2,$$

where $\dot{z}_1 = z_2 - k_1 z_1$ and $\dot{z}_2 = -k_2 z_2 - z_1 + \bar{C}(F_{e,1} + \bar{F}_e\mathrm{sgn}(z_2))$ are bounded (since $F_{e,1}$ and $\mathrm{sgn}(z_2)$ are bounded). Thus, $\dot{D}(t)$ is bounded, and $D(t)$ is uniformly continuous. By Barbalat's lemma (Slotine & Li, 1991):

$$\lim_{t\to\infty} D(t) = 0. \tag{36}$$

Hence, $z_1 \to 0$ and $z_2 \to 0$ as $t \to \infty$, ensuring $\lim_{t\to\infty} y(t) = y^d$. The controller (28) achieves global asymptotic stability despite parametric uncertainties and external disturbances.

Remark 3.1: The use of $\mathrm{sgn}(z_2)$ in (28) ensures robustness but introduces discontinuities, potentially causing chattering in u, especially near $z_2 = 0$. This limitation motivates the adaptive approach in Section 3.3.

Remark 3.2: The robust control law (28) is discontinuous, which implies that it does not satisfy the conditions necessary to guarantee the existence and uniqueness of a solution, as stated in Theorem 3.1.

In the following subsection, we leverage the structure of the approximation function (5) to integrate an NN-based approximator, facilitating the design of a robust adaptive control law that satisfies the conditions of Theorem 3.1.

3.3 Adaptive robust backstepping control via radial basis function neural network

The nominal controller (28) relies on an arbitrarily predefined upper bound $\bar{F}_e$ for system uncertainty, limiting its adaptability. To overcome this, we propose an alternative controller utilising a radial basis function neural network (RBF-NN) to estimate exogenous disturbances and discontinuous frictional forces. The lumped uncertainty, encompassing these components, is defined as $f_1(x_2) = f(x_2) + F_{e,1} - K_v x_2$, where the known viscous term $K_v x_2$ is excluded from estimation, targeting only the discontinuous $f(x_2)$ and unknown disturbances.

The RBF-NN, illustrated in Figure 1, is a three-layer architecture: the input layer processes the linear drive's two states, the hidden layer computes weighted Gaussian activation functions, and the output layer approximates the lumped disturbance. The activation function is:

$$\phi_i(x) = \exp\left\{-\sum_{k=1}^{2}\frac{(x_k - \bar{x}_{ik})^2}{\sigma_{ik}^2}\right\}, \quad i = 1, 2, \ldots, N, \tag{37}$$

where $\bar{x}_{ik}$ and σ_{ik}^2 denote the mean and variance of the Gaussian functions. This is reformulated as $\phi_i(x) = \exp\{-(x - \bar{x}_{ci})^\top Q_i$

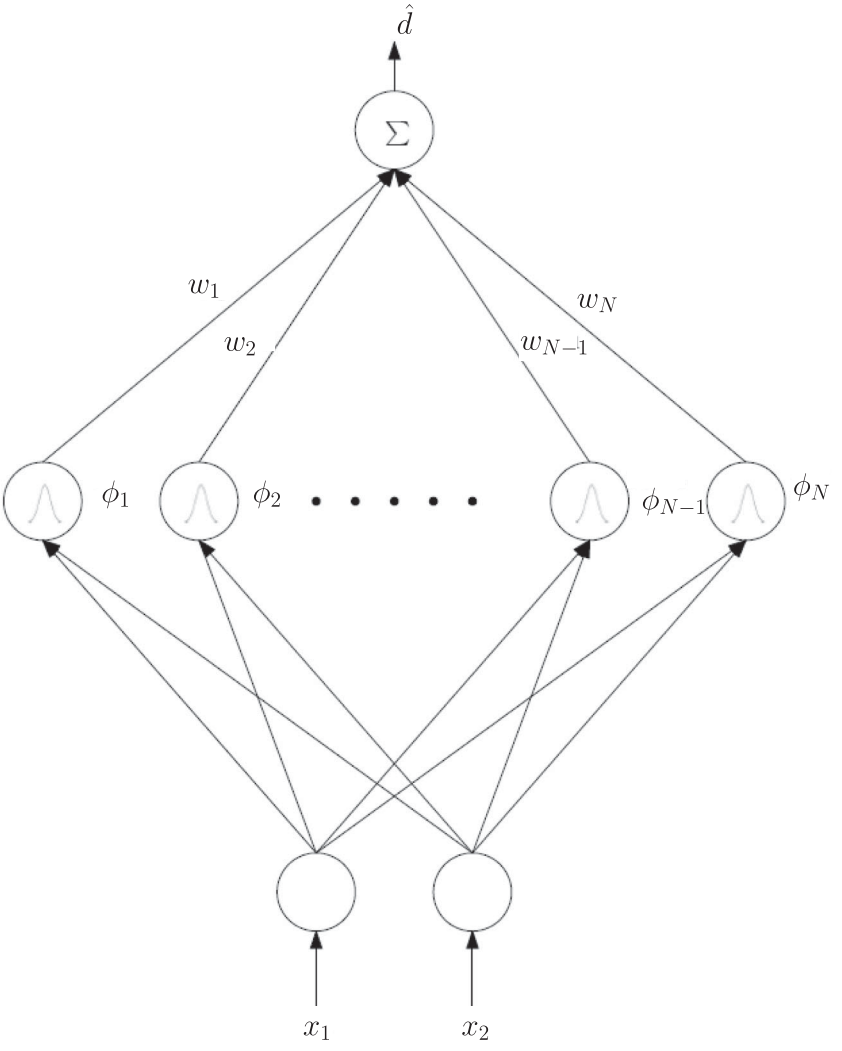

Figure 1. Configuration of the RBF-NN.

$(x - \bar{x}_{ci})\}$, with $Q_i = \text{diag}(\sigma_{i1}^{-2}, \sigma_{i2}^{-2})$ and $\bar{x}_{ci} = [\bar{x}_{i1}, \bar{x}_{i2}]^\top$. The RBF-NN output is:

$$d(x) = W^\top \Phi(x), \tag{38}$$

where $W = [w_1, w_2, \ldots, w_N]^\top$ is the weight vector, $\Phi(x) = [\phi_1(x), \phi_2(x), \ldots, \phi_N(x)]^\top$ is the activation vector, and N is the number of hidden neurons. Weights w_i are optimised via a quadratic cost function $J = \frac{1}{2}z_1^2$ based on the tracking error z_1, using supervised gradient descent (Lu et al., 2010). The RBF-NN's selection is justified by its universal approximation capability, simplicity, and rapid learning (Park & Sandberg, 1991; X. Wang et al., 2022), enabling representation of discontinuous components (5) and supporting widespread engineering applications (Ting et al., 2015).

Incorporating $f_1(x_2)$ into the dynamics (3), the system is expressed as $\dot{x}_2 = \bar{A}x_2 + \bar{B}u + \bar{C}(f_1(x_2) + K_v x_2)$. The RBF-NN approximates $f_1(x_2)$ with $d(x)$, defining the approximation error $\epsilon = f_1(x_2) - d(x)$ with $|\epsilon| \leq \bar{\epsilon}$. The adaptive estimate $\hat{\epsilon}$ and error $\tilde{\epsilon} = \hat{\epsilon} - \bar{\epsilon}$ are introduced.

The control law, integrating the RBF-NN estimate, is:

$$u = \bar{B}^{-1}\left[-k_2 z_2 - z_1 - \bar{A}x_2 - \bar{C}K_v x_2 - \bar{C}d(x) - k_r\hat{\epsilon}|\bar{C}|\arctan(cz_2) + \dot{\eta}\right], \tag{39}$$

where $k_2 > 0$, $k_r > 0$, and $c > 0$ are design parameters, with the arctan term providing smooth robust compensation. The adaptation law is:

$$\dot{\hat{\epsilon}} = \beta|\bar{C}||z_2|\arctan(cz_2)|, \quad \hat{\epsilon}(0) \geq 0, \ \ \beta > 0, \tag{40}$$

dynamically updating the uncertainty bound estimate.

Theorem 3.2 (Global Asymptotic Stability under Adaptive Robust Backstepping Control): *Consider the system in* (3)*, controlled by* (39) *and* (40)*, with tracking errors* $z_1 = y - y^d$*,* $z_2 = x_2 - \eta$*, and* $\eta = \dot{y}^d - k_1 z_1$ $(k_1 > 0)$ (22)*. If* $k_r > \frac{2}{\pi}$*, then* $z_1(t) \to 0$ *and* $z_2(t) \to 0$ *as* $t \to \infty$*, ensuring global asymptotic stability for any* $M > 0$*.*

Proof: We begin by defining a Lyapunov function to assess stability, given by

$$V = \frac{1}{2}(z_1^2 + z_2^2) + \frac{1}{2\beta}\tilde{\epsilon}^2, \tag{41}$$

where $\tilde{\epsilon} = \hat{\epsilon} - \bar{\epsilon}$ and $\beta > 0$. The time derivative of V is computed as

$$\dot{V} = z_1\dot{z}_1 + z_2\dot{z}_2 + \frac{1}{\beta}\tilde{\epsilon}\dot{\hat{\epsilon}}. \tag{42}$$

For the first term, since $\dot{z}_1 = z_2 - k_1 z_1$, we obtain

$$z_1\dot{z}_1 = z_1 z_2 - k_1 z_1^2. \tag{43}$$

Next, we derive the dynamics of z_2 using (24) and (39), resulting in

$$\dot{z}_2 = -k_2 z_2 - z_1 + \bar{C}\epsilon - k_r\hat{\epsilon}|\bar{C}|\arctan(cz_2), \tag{44}$$

where $\epsilon = f_1(x_2) - d(x)$. Multiplying by z_2 yields

$$z_2\dot{z}_2 = -k_2 z_2^2 - z_1 z_2 + z_2\bar{C}\epsilon - k_r\hat{\epsilon}|\bar{C}|z_2\arctan(cz_2). \tag{45}$$

The adaptation term from (40) gives

$$\frac{1}{\beta}\tilde{\epsilon}\dot{\hat{\epsilon}} = \tilde{\epsilon}|\bar{C}||z_2||\arctan(cz_2)|. \tag{46}$$

Combining these, and noting $\tilde{\epsilon} = \hat{\epsilon} - \bar{\epsilon}$, we arrive at

$$\dot{V} = -k_1 z_1^2 - k_2 z_2^2 + z_2\bar{C}\epsilon + |\bar{C}||z_2||\arctan(cz_2)|(-k_r\hat{\epsilon} + \tilde{\epsilon}). \tag{47}$$

To bound the uncertainty, with $\bar{C} = -1/M < 0$ and $|\epsilon| \le \bar{\epsilon}$, we get

$$\dot{V} \le -k_1 z_1^2 - k_2 z_2^2 + \frac{|z_2|}{M}\left[\bar{\epsilon} + |\arctan(cz_2)|(-k_r\hat{\epsilon} + \tilde{\epsilon})\right]. \tag{48}$$

For stability, the bracketed term must be non-positive. Substituting $\tilde{\epsilon} = \hat{\epsilon} - \bar{\epsilon}$, and at $|\arctan(cz_2)| = \frac{\pi}{2}$, we need

$$\frac{\pi}{2}(-k_r\hat{\epsilon} + \hat{\epsilon} - \bar{\epsilon}) \le -\bar{\epsilon}. \tag{49}$$

Simplifying, $\frac{\pi}{2}(-k_r\hat{\epsilon} + \hat{\epsilon} - \bar{\epsilon}) = \frac{\pi}{2}(1 - k_r)\hat{\epsilon} - \frac{\pi}{2}\bar{\epsilon} \le -\bar{\epsilon}$. Thus, $\frac{\pi}{2}(1 - k_r)\hat{\epsilon} \le \bar{\epsilon}(1 - \frac{\pi}{2})$. Since $1 - \frac{\pi}{2} < 0$, and $\hat{\epsilon} \ge 0$, we require $1 - k_r \le 0$, so $k_r \ge 1$. However, if $\hat{\epsilon} < \bar{\epsilon}$, the adaptation law $\dot{\hat{\epsilon}} > 0$ when $z_2 \ne 0$ ensures $\hat{\epsilon}$ increases. To dominate $\bar{\epsilon}$, set $k_r\hat{\epsilon}\frac{\pi}{2} \ge \bar{\epsilon}$, so $k_r \ge \frac{2}{\pi}\frac{\bar{\epsilon}}{\hat{\epsilon}}$. As $\hat{\epsilon}$ grows, $k_r > \frac{2}{\pi}$ suffices. Consequently,

$$\dot{V} \le -k_1 z_1^2 - k_2 z_2^2 \le 0. \tag{50}$$

Since $\dot{V}$ is uniformly continuous, Barbalat's lemma ensures $z_1, z_2 \to 0$, establishing global asymptotic stability. ■

Proposition 3.3: *Given the control law*

$$u = \overline{B}^{-1}\left[-k_2 z_2 - z_1 - \overline{A}x_2 - \overline{C}K_v x_2 - \overline{C}d(x) - k_r\hat{\epsilon}|\overline{C}|\arctan(cz_2) + \dot{\eta}\right], \tag{51}$$

where k_2, k_r, and c are positive design parameters, $\overline{A}$, $\overline{B}$, $\overline{C}$, and K_v are system parameters, z_1, z_2, and η are defined in the backstepping procedure, $d(x)$ is the RBF-NN output, and $\hat{\epsilon}$ is the adaptive estimate of the approximation error bound, the control law u is Lipschitz continuous with respect to the state vector $x = [x_1\ x_2]^T$.

Proof: To establish the Lipschitz continuity of the control law u, it is necessary to demonstrate the existence of a constant $L_u > 0$ such that for any state vectors $x = [x_1\ x_2]^T$ and $\tilde{x} = [\tilde{x}_1\ \tilde{x}_2]^T$ in the domain of u, the following condition holds:

$$||u(x) - u(\tilde{x})|| \le L_u||x - \tilde{x}||. \tag{52}$$

Consider the difference between the control law evaluated at two distinct state vectors x and $\tilde{x}$:

$$\begin{aligned} u(x) - u(\tilde{x}) = \overline{B}^{-1}\big[&-k_2(z_2 - \tilde{z}_2) - (z_1 - \tilde{z}_1) - \overline{A}(x_2 - \tilde{x}_2) \\ &- \overline{C}K_v(x_2 - \tilde{x}_2) - \overline{C}(d(x) - d(\tilde{x})) \\ &- k_r\hat{\epsilon}|\overline{C}|(\arctan(cz_2) - \arctan(c\tilde{z}_2)) \\ &+ (\dot{\eta} - \dot{\tilde{\eta}})\big]. \end{aligned} \tag{53}$$

We proceed to analyse each term within the equation:

(i) *Linear Terms*: The terms involving z_1, z_2, x_2, and $\dot{\eta}$ are linear in x_1 and x_2 due to the definitions of $z_1 = x_1 - y_d$, $z_2 = x_2 - \eta$, and η as a function of x_1 and x_2. Consequently, their differences, i.e. $(z_2 - \tilde{z}_2)$, $(z_1 - \tilde{z}_1)$, $(x_2 - \tilde{x}_2)$, and $(\dot{\eta} - \dot{\tilde{\eta}})$, are Lipschitz continuous with respect to x_1 and x_2. For instance, $|x_2 - \tilde{x}_2| \le ||x - \tilde{x}||$.

(ii) *RBF-NN Output Term*: The term involving the RBF-NN output is $\overline{C}(d(x) - d(\tilde{x}))$. From prior results, it is established that $d(x)$ is Lipschitz continuous, satisfying the condition:

$$||d(x) - d(\tilde{x})|| \le L_f||x - \tilde{x}||, \tag{54}$$

where L_f represents the Lipschitz constant associated with $d(x)$.

(iii) *Arctangent Term*: The term involving the arctangent function is $k_r\hat{\epsilon}|\overline{C}|(\arctan(cz_2) - \arctan(c\tilde{z}_2))$. The arctangent function, $\arctan(x)$, is inherently Lipschitz continuous, with its derivative, $\frac{1}{1+x^2}$, bounded by 1. Therefore, we have:

$$|\arctan(cz_2) - \arctan(c\tilde{z}_2)| \le c|z_2 - \tilde{z}_2|. \tag{55}$$

Given that z_2 is Lipschitz continuous with respect to x, this term is also Lipschitz continuous with respect to x.

(iv) *Adaptive Estimate Term*: The term involving the arctangent function is $k_r\hat{\epsilon}|\overline{C}|(\arctan(cz_2) - \arctan(c\tilde{z}_2))$. The arctangent function, $\arctan(x)$, is inherently Lipschitz continuous, with its derivative, $\frac{1}{1+x^2}$, bounded by 1. Therefore, we have:

$$|\arctan(cz_2) - \arctan(c\tilde{z}_2)| \le c|z_2 - \tilde{z}_2|. \tag{56}$$

Given that z_2 is Lipschitz continuous with respect to x, the term $\arctan(cz_2)$ is also Lipschitz continuous with respect to x. Furthermore, $\hat{\epsilon}$ is bounded due to the stability analysis of the adaptive system. The product of a bounded function $(\hat{\epsilon})$ and a Lipschitz continuous function $(\arctan(cz_2))$ is Lipschitz continuous. Therefore, the

term $k_r\hat{e}|\overline{C}|(\arctan(cz_2) - \arctan(c\tilde{z}_2))$ is Lipschitz continuous with respect to x.

By synthesising these results and applying the triangle inequality, it is feasible to identify a constant L_u such that:

$$||u(x) - u(\tilde{x})|| \leq L_u||x - \tilde{x}||. \tag{57}$$

This confirms that the control law u satisfies the Lipschitz continuity condition with respect to the state vector x. ■

4. Simulation results

The linear drive system is simulated using the robust backstepping controller (R-BSC) (28) and the proposed adaptive robust backstepping controller (AR-BSC) under different conditions in the presence of disturbances. To benchmark the proposed controller, we also implement the fast nonsingular terminal sliding mode controller (FTNSMC) developed by Zheng et al. (2015), alongside the R-BSC and the adaptive recursive terminal sliding mode controller (ARTSMC) from Qin et al. (2024). The FTNSMC is selected due to its ability to achieve fast convergence and robustness against uncertainties, making it a suitable comparison for our nonlinear linear motor drive system.

All simulations were conducted in MATLAB/Simulink, implementing the linear drive system model and control laws as described in Sections 2 and 3, with performance metrics calculated numerically based on the simulated position and control input data.

The control scheme (FTNSMC), proposed in Zheng et al. (2015) is given by

$$u^{\text{SMC}} = u_0 + u_1, \tag{58}$$

where u_0 is the nominal control input derived from the plant model assuming no uncertainties, and u_1 is a reaching control law designed to drive the system states onto the sliding surface and handle disturbances. For consistency with our notation, we define $r \triangleq y^d$ as the desired reference position trajectory, such that $\dot{r} = \dot{y}^d$ and $\ddot{r} = \ddot{y}^d$ represent the reference velocity and acceleration, respectively. These control signals are explicitly expressed as follows:

$$u_0 = M\ddot{y}^d + f' - \frac{M}{\lambda\gamma}\text{sign}(\dot{z}_1)^{2-\gamma}, \tag{59}$$

where $f' = Bx_2 + f(x_2)$, $\lambda > 0$, $1 < \gamma < 2$, and the notation $\text{sign}(x)^a = |x|^a\text{sign}(x)$ defines a fractional power of the sign function. The reaching control law is given by

$$u_1 = M[k_1's + k_2'\text{sign}(s)^\rho], \tag{60}$$

where $k_1', k_2' > 0$, $0 < \rho < 1$, and the sliding variable s is defined as

$$s = z_1 + \lambda\text{sign}(\dot{z}_1)^\gamma, \tag{61}$$

with $z_1 = y - y^d = x_1 - y^d$ being the position tracking error, consistent with our earlier definition in Section 3.1.

For the simulation study, the parameters are set as $\gamma = 1.4$, $\rho = 0.8$, and $\lambda = 0.016$, following the selection in Zheng et al. (2015) to ensure fast convergence and reduced chattering. The gains $k_1' = 500$ and $k_2' = 200$ are chosen as they provide improved tracking performance and robustness for the linear motor studied in this work, determined through tuning to balance accuracy and control effort.

Additionally, we implement the ARTSMC scheme proposed by Qin et al. (2024). In what follows, we present the simulation results.

Two case studies are considered, incorporating parameter variations and external disturbances, as follows:

$$\begin{aligned}&\text{Case1}: \Delta B = B, \quad f_d = \begin{cases} 0\text{ N}, & \text{for } t < 10\text{ s}, \\ 10\text{ N}, & \text{for } t \geq 10\text{ s}. \end{cases} \\ &\text{Case2}: \Delta B = 4B, \quad f_d = 15\sin(2t)\text{ N}. \end{aligned} \tag{62}$$

The parameters of the linear drive system with a mover are given as follows (Paul et al., 2022) $M = 0.3$ kg, $B = 0.7954$ N·s/m, and $k_f = 1$ N/V. The frictional force parameters are given as $f_c = 0.006$, $f_s = 0.01$, $\dot{x}_s = 0.1$, and $K_v = 5$.

The adaptation law is implemented alongside the AR-BSC control signal, which is derived from the Lyapunov stability theorem. Consequently, the stability of the closed-loop system is ensured. The RBF-NN is implemented by randomly initialising the weights. Additionally, the parameters of the backstepping control system are set as:

$$k_1 = 40, \quad k_2 = 40, \quad \beta = 1, \quad \bar{F}_e = 20. \tag{63}$$

The sign function in the FTNSMC control law introduces discontinuities. Since a continuous control signal is desirable for practical applications, an approximation of this function is used. Various approximation methods can be employed; in this work, we adopt the following approximation of the sign function (Paul et al., 2022) for the nominal controller (28):

$$\text{sign}(x_2) \approx \frac{2}{\pi}\arctan\left(900\frac{2}{\pi}x_2\right). \tag{64}$$

To quantitatively compare the performances of the controllers, we employ two tracking performance metrics: the Root Mean Square Error (RMSE), defined as $\text{RMSE} = \sqrt{\frac{1}{t_f}\int_0^{T_f}(y - y^d)^2\,\text{d}t}$, which measures the average magnitude of the tracking errors, and the Maximum Absolute Error (MAE), given by $\text{MAE} = \max|y - y^d|$, which captures the largest deviation between the simulated and reference positions. Additionally, input chattering is assessed using the following metric:

$$\text{Total Chattering} = \int_0^{T_f} |\dot{u}|\,\text{d}t. \tag{65}$$

where T_f is the final time of the simulations.

Remark 4.1: The input chattering metric (65) is a standard method for quantifying the *total variation of the control input* over time. It corresponds to the L_1-norm of the control input's derivative and effectively captures the energy associated with high-frequency switching, which characterises chattering (Levant, 2010). Energy-based measures provide a systematic approach to evaluating the smoothness of control signals while

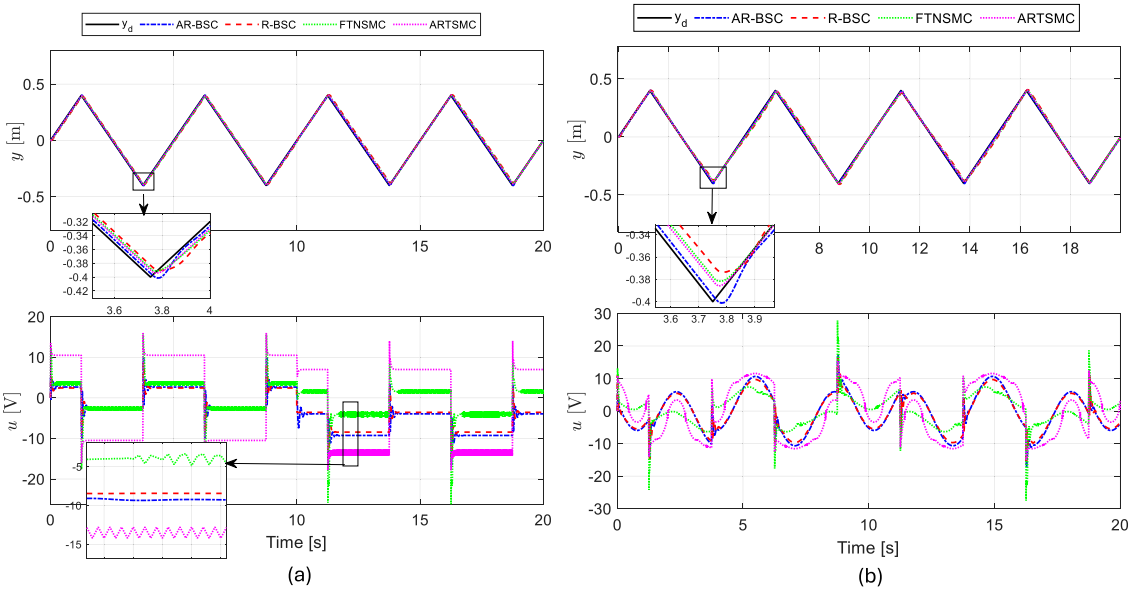

Figure 2. Triangular position reference tracking with disturbance occurring at $t \geq 10$ s. (a) Case 1: Results showing the position tracking (top) and control signal (bottom) under constant-type disturbance. (b) Case 2: Results showing the position tracking (top) and control signal (bottom) under time-varying disturbance.

mitigating inaccuracies from direct observations. Levant (2010) formalises chattering as energy dissipation caused by switching forces, which can be associated with virtual dry friction and accumulated over time. By integrating $|\dot{u}|$, the chattering metric ensures that both the magnitude and frequency of control input variations are accounted for, making it a reasonable and reliable measure for assessing and comparing chattering phenomena in practical systems. This approach aligns with the classification of chattering into infinitesimal, bounded, and unbounded types (Levant, 2010), ensuring its theoretical validity and practical relevance.

Two types of reference tracking are considered. The first is a periodic triangular reference trajectory, while the second is a periodic sinusoidal reference for the mover position. These trajectories are chosen as they represent repetitive motion tasks, a common characteristic of linear motor-driven systems. For instance, surface mount equipment and glue dispensing machines must consistently execute the same motion for each batch of products on the production line while ensuring sustained high precision and stable performance over time (Z. Liu et al., 2024).

The selected trajectories illustrate two distinct scenarios: the periodic sinusoidal trajectory represents cases where the reference is continuous with smooth transitions, whereas the triangular reference represents periodic linear motions with sharp transitions.

In each case study, we compare the proposed backstepping controller with FTNSMC and ARTSMC. The parameters for AR-BSC are set to $\hat{\epsilon}(0) = 2.1/\pi$ and $k_f = 50$. Other than these differences, all controllers are implemented under identical conditions for fair benchmarking. The position tracking and required input voltage results are shown in Figures 2 and 4. Additionally, the tracking errors for the triangular and sinusoidal trajectories are presented in Figures 3 and 5, respectively.

In Case 1 (Figure 2(a)), under the triangular reference position, all controllers exhibited good tracking performance before the constant disturbance was introduced into the system at $t = 10$ s. However, the performance of the R-BSC degraded significantly once the nonzero constant disturbance was applied, whereas AR-BSC, FTNSMC, and ARTSMC demonstrated robustness. The inferior performance of R-BSC can be attributed to its simplistic adaptation to disturbances within predefined bounds, unlike AR-BSC, FTNSMC, and ARTSMC, which effectively minimise variations in the control signal upon disturbance entry. It is important to highlight that the proposed AR-BSC provided a smooth control signal, while FTNSMC and ARTSMC exhibited significant input voltage chattering.

In Case 2 (Figure 2(b)), R-BSC showed the poorest tracking performance in the presence of a sinusoidal disturbance, whereas AR-BSC closely matched the performance of ARTSMC. Moreover, AR-BSC provided the smoothest control signal response but with higher magnitudes compared to R-BSC and FTNSMC. Tracking errors for both cases are presented in Figure 3, with R-BSC demonstrating comparatively poor performance.

For the triangular reference trajectory, the performance metrics are computed based on the errors shown in Figure 3 and presented in Table 1. The AR-BSC controller consistently outperforms the others, particularly in Case 1, where it achieves the lowest RMSE (0.0066 m) and significantly reduces chattering (0.191 kV). This demonstrates superior tracking accuracy and smoother control action.

The ARTSMC controller also exhibits competitive performance, particularly in reducing RMSE and MAE, but it lags behind AR-BSC in minimising chattering. The R-BSC controller has the highest RMSE and MAE, indicating poor tracking performance, especially in Case 1. While FTNSMC delivers reasonable accuracy, its chattering is excessively high (1.529 kV),

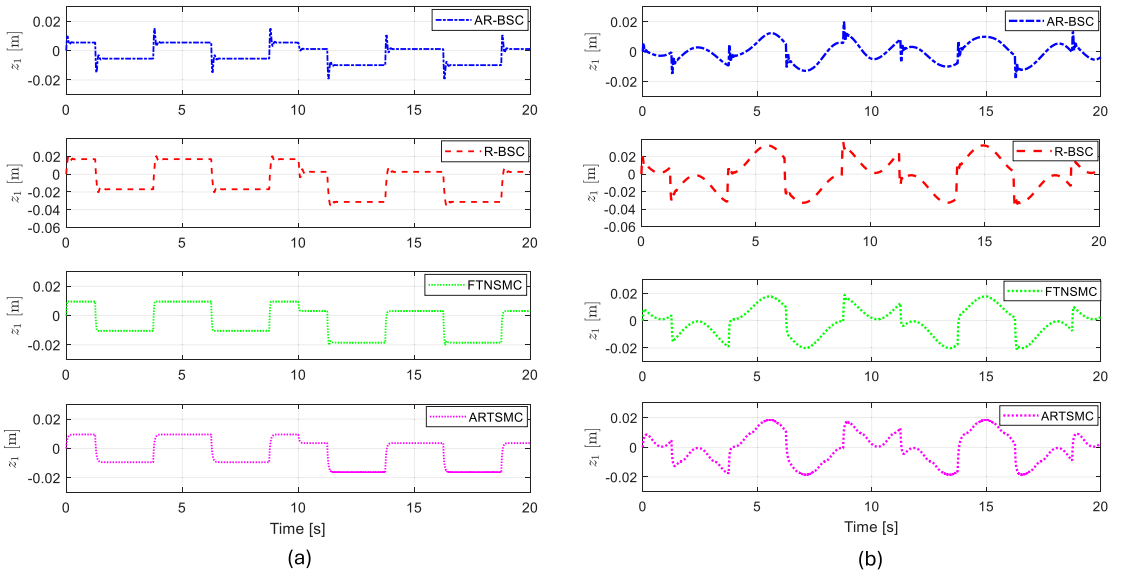

Figure 3. Triangular position reference tracking. (a) Case 1: Evolution of sampled error signals under constant-type disturbances (b) Case 2: Evolution of sampled error signals under time-varying disturbance.

Table 1. Performance comparison of controllers in terms of RMSE, MAE, and total chattering under different reference trajectories.

		Controllers			
Scenario	Performance metric	AR-BSC	R-BSC	FTNSMC	ARTSMC
Triangular reference (Case 1)	RMSE [m]	**0.0066**	0.0196	0.0116	0.0105
	MAE [m]	0.0199	0.0374	0.0210	**0.0178**
	Chattering [kV]	**0.191**	0.296	1.529	0.987
Triangular reference (Case 2)	RMSE [m]	**0.0200**	0.0240	0.0201	0.0212
	MAE [m]	**0.0206**	0.0360	0.0210	0.0207
	Chattering [kV]	**0.408**	0.524	0.465	0.859
Sinusoidal reference (Case 1)	RMSE [m]	**0.0145**	0.0227	0.0198	0.0179
	MAE [m]	0.0321	0.0389	0.0325	**0.0320**
	Chattering [kV]	**0.522**	1.258	1.129	0.971
Sinusoidal reference (Case 2)	RMSE [m]	**0.0148**	0.0243	0.0200	0.0188
	MAE [m]	0.0316	0.0423	0.0327	**0.0296**
	Chattering [kV]	**0.602**	1.299	1.212	0.940

making it less desirable for applications requiring smooth control. Overall, AR-BSC proves to be the most effective controller for this scenario, achieving a balance between accuracy and chattering reduction.

In Figure 4, the tracking performance of the studied controllers for the sinusoidal reference trajectory is shown. Similar to the previous case, R-BSC, AR-BSC, FTNSMC, and ARTSMC are compared for both Case 1 and Case 2.

In Case 1, all controllers demonstrate effective tracking performance in the absence of external disturbances. However, the proposed AR-BSC exhibits slightly superior tracking performance compared to the other three controllers. The performance of R-BSC deteriorates the most when a constant disturbance is introduced into the system, as shown in Figure 4.

In Case 2 (Figure 4(b)), the robustness of the proposed AR-BSC is further demonstrated, as it remains closely aligned with the reference trajectory despite the presence of disturbances. This point is more evident in the error plots shown in Figure 5. Additionally, it is observed that the control voltage required by ARTSMC is generally larger in magnitude than that of the other three controllers. The performance metrics for the sinusoidal reference trajectory scenarios are calculated using the error plots displayed in Figure 5, with the results detailed in Table 1. The comparison of the four controllers–AR-BSC, R-BSC, FTNSMC, and ARTSMC–reveals that AR-BSC consistently delivers superior performance in terms of tracking accuracy, achieving the lowest RMSE and MAE in both case studies. However, it is noted that ARTSMC slightly outperforms the proposed AR-BSC in terms of MAE, as the latter tends to exhibit a larger initial tracking error. AR-BSC also significantly reduces chattering, particularly in Case 1, where it outperforms all other controllers. ARTSMC demonstrates competitive performance, especially in minimising chattering in Case 2, while maintaining relatively low tracking errors. FTNSMC achieves moderate tracking accuracy but is hindered by higher chattering levels. R-BSC consistently underperforms, showing the highest error values and chattering among the controllers. Overall, AR-BSC and ARTSMC emerge as the most effective controllers, with AR-BSC demonstrating a slight advantage in most scenarios.

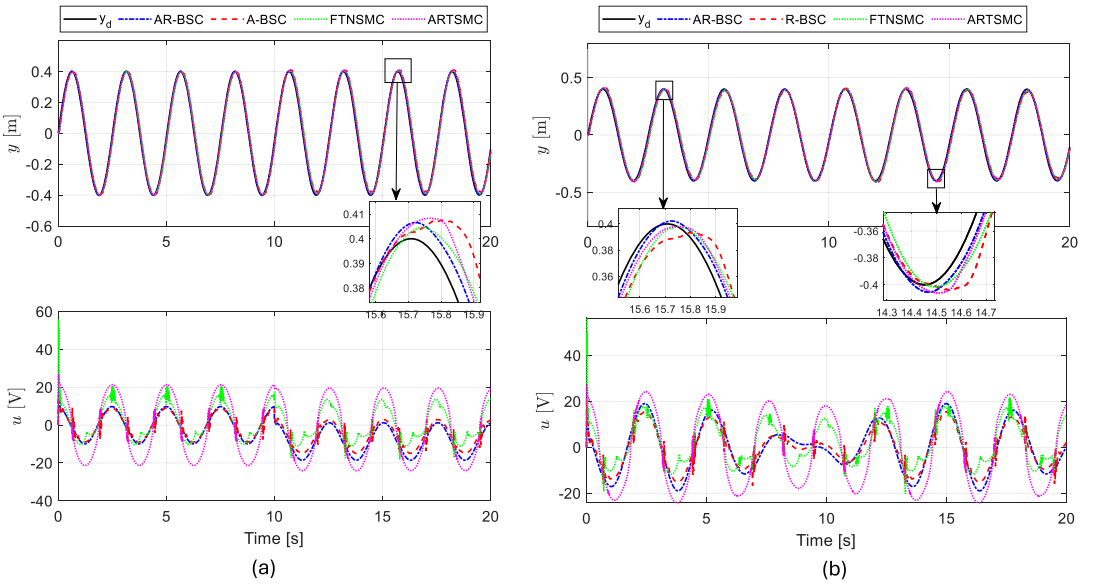

Figure 4. Sinusoidal position reference tracking. (a) Case 1: Results showing the position tracking (top) and control signal (bottom). (b) Case 2: Results showing the position tracking (top) and control signal (bottom).

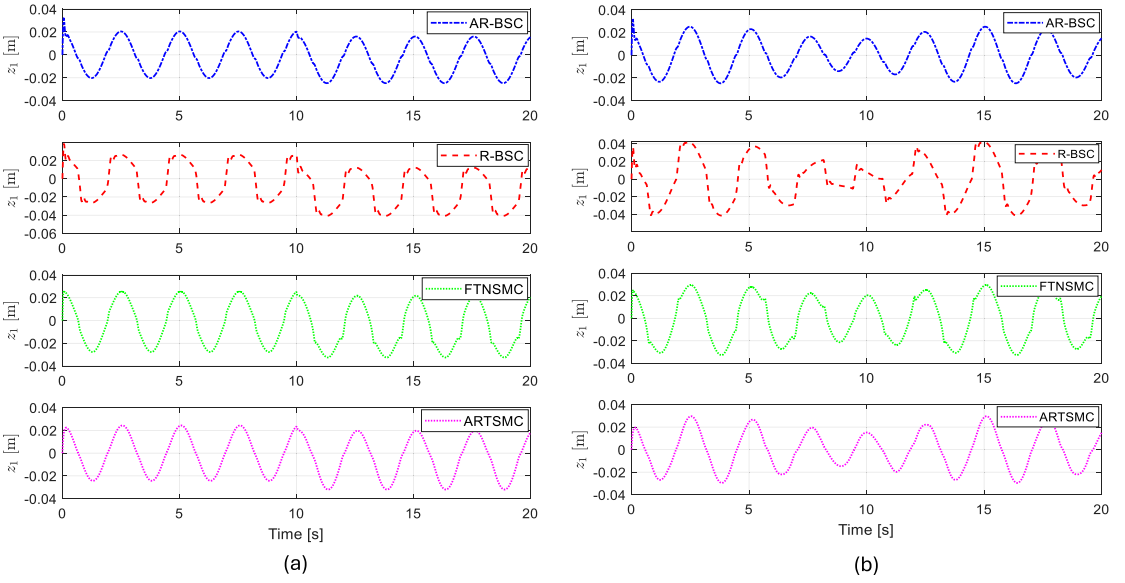

Figure 5. Sinusoidal position reference tracking. (a) Case 1: Evolution of sampled error signals (b) Case 2: Evolution of sampled error signals.

5. Conclusions

This paper has presented a novel backstepping control system with a stability guarantee that advances position control for linear drive systems. By integrating AR-BSC with an RBF-NN, our approach addresses practical challenges such as parameter uncertainty, discontinuous frictional forces, and external disturbances, outperforming traditional methods by providing precise tracking and minimal chattering–key requirements for real-world precision applications. A robust control scheme that relies on the disturbance upper bound for its implementation is first proposed. However, since this approach may lead to conservative performance and fail to accurately capture disturbance dynamics, we introduce an adaptive robust backstepping controller. This controller employs a RBF-NN, which is easy to train and implement, to approximate the lumped disturbances affecting the linear drive system. The adaptive scheme relies on the RBF-NN to approximate lumped disturbances, including discontinuous frictional forces. The characteristics of the approximation function are used to demonstrate that the proposed adaptive control law ensures the existence and uniqueness of the solution for the nonlinear model of the linear motor drive system.

The simulation results demonstrated that the adaptive backstepping control system provides improved performance over the robust controller with a constant upper bound defined on the external disturbance. It was also shown that the proposed scheme provides a smoother control signal and comparable tracking performance to a fast nonsingular terminal sliding mode controller. A limitation of this work is that while the

control law assumes the estimation error is always bounded, this condition is not theoretically guaranteed by the RBF-NN employed. Consequently, future research will focus on addressing this issue and performing experimental validation.

Disclosure statement

No potential conflict of interest was reported by the author(s).

ORCID

Isah A. Jimoh http://orcid.org/0000-0002-4931-9106
Ibrahim Küçükdemiral http://orcid.org/0000-0003-0174-5680

References

Ager, P., Jimoh, I. A., Bevan, G., & Küçükdemiral, I. (2024). Robust backstepping controllers for linear motor drives. In *IEEE Conference on Control Technology and Applications (CCTA)* (pp. 1–6). IEEE.

Gai, H., Li, X., Jiao, F., Cheng, X., Yang, X., & Zheng, G. (2021). Application of a new model reference adaptive control based on PID control in CNC machine tools. *Machines*, *9*(11), 274. https://doi.org/10.3390/machines9110274

Gao, H., Liu, Y., Sun, W., & Yu, X. (2023). Adaptive wavelet tracking control of dual-linear-motor-driven gantry stage with suppression of crossbeam rotation. *IEEE/ASME Transactions on Mechatronics*, *29*(1), 97–105. https://doi.org/10.1109/TMECH.2023.3293568

Gwiazda, P., Lorenz, T., & Marciniak-Czochra, A. (2010). A nonlinear structured population model: Lipschitz continuity of measure-valued solutions with respect to model ingredients. *Journal of Differential Equations*, *248*(11), 2703–2735. https://doi.org/10.1016/j.jde.2010.02.010

Levant, A. (2010). Chattering analysis. *IEEE Transactions on Automatic Control*, *55*(6), 1380–1389. https://doi.org/10.1109/TAC.2010.2041973

Li, L., Pei, G., Liu, J., Du, P., Pei, L., & Zhong, C. (2020). 2-DOF robust H_∞ control for permanent magnet synchronous motor with disturbance observer. *IEEE Transactions on Power Electronics*, *36*(3), 3462–3472. https://doi.org/10.1109/TPEL.63

Li, Y., Zheng, L., Liang, Y., & Yu, Y. (2020). Adaptive compensation control of an electromagnetic active suspension system based on nonlinear characteristics of the linear motor. *Journal of Vibration and Control*, *26*(21-22), 1873–1885. https://doi.org/10.1177/1077546320909985

Lin, F. J., Wai, R. J., Chou, W. D., & Hsu, S. P. (2002). Adaptive backstepping control using recurrent neural network for linear induction motor drive. *IEEE Transactions on Industrial Electronics*, *49*(1), 134–146. https://doi.org/10.1109/41.982257

Liu, Z., Gao, H., Yu, X., Lin, W., Qiu, J., Rodríguez-Andina, J. J., & Qu, D. (2023). B-spline wavelet neural-network-based adaptive control for linear-motor-driven systems via a novel gradient descent algorithm. *IEEE Transactions on Industrial Electronics*, *71*(2), 1896–1905. https://doi.org/10.1109/TIE.2023.3260318

Liu, Z., Yu, X., Lin, W., & Rodríguez-Andina, J. J. (2024). Iterative learning observer-based high-precision motion control for repetitive motion tasks of linear motor driven systems. *IEEE Open Journal of the Industrial Electronics Society*, *5*, 54–66. https://doi.org/10.1109/OJIES.2024.3359951

Lu, H. C., Tsai, C. H., & Chang, M. H. (2010). Radial basis function neural network with sliding mode control for robotic manipulators. In *2010 IEEE International Conference on Systems, Man and Cybernetics* (pp. 1209–1215). IEEE. https://doi.org/10.1109/ICSMC.2010.5642384

Mirić, S., Giuffrida, R., Bortis, D., & Kolar, J. W. (2020). Dynamic electromechanical model and position controller design of a new high-precision self-bearing linear actuator. *IEEE Transactions on Industrial Electronics*, *68*(1), 744–755. https://doi.org/10.1109/TIE.41

Mohanraj, D., Aruldavid, R., Verma, R., Sathiyasekar, K., Barnawi, A. B., Chokkalingam, B., & Mihet-Popa, L. (2022). A review of BLDC motor: state of art, advanced control techniques, and applications. *IEEE Access*, *10*, 54833–54869. https://doi.org/10.1109/ACCESS.2022.3175011

Mousavi, Y., Bevan, G., Kucukdemiral, I. B., & Fekih, A. (2023). Observer-based high-order sliding mode control of DFIG-based wind energy conversion systems subjected to sensor faults. *IEEE Transactions on Industry Applications*, *60*(1), 1750–1759. https://doi.org/10.1109/TIA.2023.3317823

Nakata, Y., & Noda, T. (2023). Fusion hybrid linear actuator: Concept and disturbance resistance evaluation. *IEEE/ASME Transactions on Mechatronics*, *28*(4), 2167–2177. https://doi.org/10.1109/TMECH.2023.3237725

Otten, G., De Vries, T. J., Van Amerongen, J., Rankers, A. M., & Gaal, E. W. (1997). Linear motor motion control using a learning feedforward controller. *IEEE/ASME Transactions on Mechatronics*, *2*(3), 179–187. https://doi.org/10.1109/3516.622970

Park, J., & Sandberg, I. W. (1991). Universal approximation using radial-basis-function networks. *Neural Computation*, *3*(2), 246–257. https://doi.org/10.1162/neco.1991.3.2.246

Paul, A., Küçükdemiral, I., & Bevan, G. (2022). Nonlinear model predictive motion control of linear motor drive for micro/nano-positioning applications. In *2022 4th International Conference on Electrical, Control and Instrumentation Engineering (ICECIE)* (pp. 1–7). IEEE.

Qin, Y., Chen, Q., & Ming, C. (2024). Adaptive recursive sliding mode based trajectory tracking control for cable-driven continuum robots. *ISA Transactions*, *147*, 501–510. https://doi.org/10.1016/j.isatra.2024.02.016

Shao, K., Zheng, J., Wang, H., Wang, X., Lu, R., & Man, Z. (2021). Tracking control of a linear motor positioner based on barrier function adaptive sliding mode. *IEEE Transactions on Industrial Informatics*, *17*(11), 7479–7488. https://doi.org/10.1109/TII.2021.3057832

Shao, K., Zheng, J., Wang, H., Xu, F., Wang, X., & Liang, B. (2021). Recursive sliding mode control with adaptive disturbance observer for a linear motor positioner. *Mechanical Systems and Signal Processing*, *146*, 107014. https://doi.org/10.1016/j.ymssp.2020.107014

Shi, X., & Chen, Y. (2023). Extended state observer design with fractional order Bode's ideal cut-off filter in a linear motor motion control system. *Proceedings of the Institution of Mechanical Engineers, Part I: Journal of Systems and Control Engineering*, *237*(2), 196–206. https://doi.org/10.1177/09544089221102417

Slotine, J. J. E., & Li, W. (1991). *Applied nonlinear control* (Vol. 199, No. 1). Prentice-Hall, England.

Sun, G., Wu, L., Kuang, Z., Ma, Z., & Liu, J. (2018). Practical tracking control of linear motor via fractional-order sliding mode. *Automatica*, *94*, 221–235. https://doi.org/10.1016/j.automatica.2018.02.011

Sun, X., Zhu, Y., Cai, Y., Yao, M., Sun, Y., & Lei, G. (2023). Optimized-sector-based model predictive torque control with sliding mode controller for switched reluctance motor. *IEEE Transactions on Energy Conversion*, *39*(1), 379–388. https://doi.org/10.1109/TEC.2023.3301000

Ting, C. S., Chang, Y. N., Shi, B. W., & Lieu, J. F. (2015). Adaptive backstepping control for permanent magnet linear synchronous motor servo drive. *IET Electric Power Applications*, *9*(3), 265–279. https://doi.org/10.1049/elp2.v9.3

Tu, W., & Dong, J. (2023). Robust sliding mode control for a class of nonlinear systems through dual-layer sliding mode scheme. *Journal of the Franklin Institute*, *360*(13), 10227–10250. https://doi.org/10.1016/j.jfranklin.2023.07.019

Van Den Braembussche, P., Swevers, J., Van Brussel, H., & Vanherck, P. (1996). Accurate tracking control of linear synchronous motor machine tool axes. *Mechatronics*, *6*(5), 507–521. https://doi.org/10.1016/0957-4158(95)00090-9

Wallscheid, O. (2021). Thermal monitoring of electric motors: State-of-the-art review and future challenges. *IEEE Open Journal of Industry Applications*, *2*, 204–223. https://doi.org/10.1109/OJIA.2021.3091870

Walter, W. (2013). *Ordinary differential equations*. (Vol. 182). Springer Science & Business Media.

Wang, X., Chen, F., Zhu, R., Huang, X., Sang, N., Yang, G., & Zhang, C. (2021). A review on disturbance analysis and suppression for permanent magnet linear synchronous motor. *Actuators*, *10*(4), 77. https://doi.org/10.3390/act10040077

Wang, Z., Hu, C., Zhu, Y., He, S., Yang, K., & Zhang, M. (2017). Neural network learning adaptive robust control of an industrial linear motor-driven stage with disturbance rejection ability. *IEEE Transactions on Industrial Informatics*, *13*(5), 2172–2183. https://doi.org/10.1109/TII.9424

Wang, X., Huang, T., & Chakrabarti, P. (2022). Adaptive RBF neural network control for nonlinear system. In *Complex systems: Spanning*

control and computational cybernetics: Foundations: Dedicated to Professor Georgi M. Dimirovski on his anniversary (pp. 435–455). Springer.

Wang, W., Tian, W., Wang, Z., Hua, W., & Cheng, M. (2020). A fault diagnosis method for current sensors of primary permanent-magnet linear motor drives. *IEEE Transactions on Power Electronics*, *36*(2), 2334–2345. https://doi.org/10.1109/TPEL.2020.3011125

Wang, W., Wu, J., & Chen, W (2025). The characteristics method to study global exponential stability of delayed inertial neural networks. *Mathematics and Computers in Simulation*, *232*, 91–101. https://doi.org/10.1016/j.matcom.2024.12.021

Wang, W., Zeng, W., & Chen, W (2025). Global exponential stability of periodic solutions for inertial delayed BAM neural networks. *Communications in Nonlinear Science and Numerical Simulation*, *145*, 108728. https://doi.org/10.1016/j.cnsns.2025.108728

Xu, D., Wang, B., Zhang, G., Wang, G., & Yu, Y. (2018). A review of sensorless control methods for AC motor drives. *CES Transactions on Electrical Machines and Systems*, *2*(1), 104–115. https://doi.org/10.23919/TEMS.2018.8326456

Yang, M., Fu, M., & Zhang, Z. (2021). The adoption of digital technologies in supply chains: Drivers, process and impact. *Technological Forecasting and Social Change*, *169*, 120795. https://doi.org/10.1016/j.techfore.2021.120795

Yang, H., & Liu, J. (2018). An adaptive RBF neural network control method for a class of nonlinear systems. *IEEE/CAA Journal of Automatica Sinica*, *5*(2), 457–462. https://doi.org/10.1109/JAS.2017.7510820

Yao, B., & Xu, L. (2002). Adaptive robust motion control of linear motors for precision manufacturing. *Mechatronics*, *12*(4), 595–616. https://doi.org/10.1016/S0957-4158(01)00008-3

Yu, C., Jiang, J., Zhen, Z., Bhatia, A. K., & Wang, S. (2020). Adaptive backstepping control for air-breathing hypersonic vehicle subject to mismatched uncertainties. *Aerospace Science and Technology*, *107*, 106244. https://doi.org/10.1016/j.ast.2020.106244

Yuan, M., Chen, Z., Yao, B., & Liu, X. (2019). Fast and accurate motion tracking of a linear motor system under kinematic and dynamic constraints: An integrated planning and control approach. *IEEE Transactions on Control System Technology*, *29*(2), 804–811. https://doi.org/10.1109/TCST.87

Zhang, B., Cao, R., & Hou, Z. (2020). The model-free adaptive cross-coupled control for two-dimensional linear motor. *Transactions of the Institute of Measurement and Control*, *42*(5), 1059–1069. https://doi.org/10.1177/0142331219881830

Zhang, J., Wang, H., Cao, Z., Zheng, J., Yu, M., Yazdani, A., & Shahnia, F. (2020). Fast nonsingular terminal sliding mode control for permanent-magnet linear motor via ELM. *Neural Computing and Applications*, *32*(18), 14447–14457. https://doi.org/10.1007/s00521-019-04502-4

Zheng, J., Wang, H., Man, Z., Jin, J., & Fu, M. (2015). Robust motion control of a linear motor positioner using fast nonsingular terminal sliding mode. *IEEE/ASME Transactions on Mechatronics*, *20*(4), 1743–1752. https://doi.org/10.1109/TMECH.2014.2352647